Production Engineering (2020) 14:95–104
https://doi.org/10.1007/s11740-019-00936-w

QUALITY ASSURANCE

Efficient characterization tools for deformation-induced damage at different scales

Carl F. Kusche[1] · Anthony Dunlap[2] · Felix Pütz[3] · Chunhua Tian[4] · Christoph Kirchlechner[4] · Anke Aretz[1] · Alexander Schwedt[1] · Talal Al-Samman[1] · Sebastian Münstermann[3] · Sandra Korte-Kerzel[1]

Received: 31 July 2019 / Accepted: 11 November 2019 / Published online: 23 November 2019

Abstract
In modern multiphase materials, damage initiation and growth during plastic deformation is a commonly observed and technologically relevant process. To reliably assess the state of damage in a specimen or, ultimately, a formed product, precise and comparable damage quantification is required. Furthermore, the key to understanding the initiation and evolution of voids in such materials is the characterization of the initiating microstructural mechanisms in a statistically relevant way over a large number of damage sites. In this work, we present the results of large-scale scanning electron microscopy methods for automated damage recognition and analytical characterization, together with a concept for joining the available void size statistics to micromechanical experiments such as micro-cantilever tests. These tests are able to determine a critical crack length for various types of void initiation processes, leading to an improved understanding of the consequences of ductile damage evolution and void growth, and their subsequent interaction leading to material failure. In this way, a framework for quantification and high-resolution characterization of damage mechanisms is constructed, enabling new insights on damage evolution in forming processes.

Keywords Damage · Electron microscopy · Machine learning · Characterization · Void recognition

1 Introduction

Damage-tolerant design for both forming processes and the applied materials has gained substantial interest in recent years. This is largely due to the rise in demand for high-strength materials that equally incorporate good ductility and formability, which is commonly addressed by the use of multi-phase materials [1]. For modern steels, these favourable properties are achieved by the class of advanced high strength steels (AHSS) that covers TRIP (transformation-induced plasticity) and TWIP (twinning-induced plasticity) steels, as well as dual- and complex-phase steels [2]. In the context of automative applications, the main driving force for this development is the ongoing search for materials that enable a weight reduction in crash-relevant components, while maintaining strength and ductility for optimum formability and performance [3]. However, the complex, multi-phase microstructures lead to a high internal mechanical contrast during plastic deformation. Especially in the field of dual-phase steels, extensive research has been done to understand the principles of initiation and evolution of voids during deformation [4–7]. In addition to the microstructural processes that originate in the variations of mechanical properties between different phases, microscale voids can also occur at non-metallic inclusions [8]. Understanding damage formation processes during forming is essential for assessing a product's properties as well as estimating and enhancing the expected service life time.

While efficient characterization to quantify the damage-induced degradation of mechanical properties is possible by testing macro-scale specimens or even formed parts [9], direct characterization of the microscale voids induced during deformation using microscopy requires

✉ Carl F. Kusche
kusche@imm.rwth-aachen.de

1 Institute for Physical Metallurgy and Materials Physics, RWTH Aachen University, Aachen, Germany

2 Central Facility for Electron Microscopy, RWTH Aachen University, Aachen, Germany

3 Steel Institute, RWTH Aachen University, Aachen, Germany

4 Max-Planck-Institut für Eisenforschung GmbH, Düsseldorf, Germany

high resolution imaging of the material. To reliably quantify damage in a deformed specimen large fields of view are required to deliver an assessment backed by sufficient statistical relevance. Damage characterization for dual-phase steels has extensively been performed in terms of determining the underlying microstructural mechanisms, namely the cracking of martensite islands, and the decohesion of interfaces between ferrite and martensite as well as at ferrite grain boundaries [8, 10]. As the interplay of these mechanisms is typically complex, a large fraction of voids will evolve based on several of these mechanisms including both brittle and ductile mechanisms, such as in the plastic flow of ferrite around a martensite crack [11, 12]. Additionally, agglomeration of voids in microstructural features at larger scales, such as martensite bands, has to be considered [7].

While X-ray tomography is frequently used in the context of damage void analysis, this technique is typically limited in terms of spatial resolution and investigated volumes, with void sizes of the order of 5 µm detectable in X-ray microtomography [13, 14], sub-µm resolution is attainable in X-ray nanotomography and using synchrotron radiation [14, 15]. However, in both cases, limitations in sample size may prevent statistically relevant analysis of all emerging microstructural damage events [15]. SEM-based solutions therefore deliver the highest spatial resolution for quantifying individual void sizes, while, coupled to modern image processing and recognition tools, maintain a large field of view through automated image acquisition and void recognition. Microstructural features like the martensite distribution in the microstructure can be evaluated using image recognition tools [16]. Analytical detectors like EBSD and EDX additionally enable the further analysis of the interplay of microstructure and voids. In principle, these methods can also be extended to the third dimension using mechanical or ion beam based thinning techniques, such as for example 3D EBSD, although these methods are very time consuming and, in contrast to X-ray tomography, intrinsically desctructive [17].

From these methods, statistics about present void sizes, mechanisms and geometries in the microstructure can be correlated with microscale deformation experiments, such as micro-cantilevers, micro-pillars and nanoindentation. These yield information about the local plasticity, fracture or decohesion behavior of individual phases and interfaces [18–20]. In addition, their application at different strain rates and temperatures permits the extraction of constitutive equations and identification of the underlying deformation mechanisms [21–24]. Based on the findings of these advanced tools for characterizing microstructural features as well as damage initiation processes, several modeling approaches have been implemented to simulate material deformation and damage behavior [25, 26].

In this work, we propose a framework of automated microscopy methods to gain multi-scale information about damage during forming ranging from damage quantification over identification of the dominant damage mechanisms to understanding these individual mechanisms of void initiation at the scale of plasticity and fracture of individual phases and interfaces. Two approaches based on scanning electron microscopy (SEM) are presented here incorporating automated imaging, void detection, void classification and quantification over large sample areas of the scale of a mm^2. The two methods are complementary in their analysis with both separating voids caused by inclusions from those induced by deformation, but one relying on analytical determination of inclusion composition via EDX and the other classifying detected voids regarding their nucleation mechanisms using convolutional neural networks. The statistically relevant, yet microscopically resolved damage characterization from both of these methods is compared with results typically obtained by light microscopy. While application of high resolution, large scale testing is shown to provide much more information with respect to the underlying damage mechanisms compared with light microscopy, ultimately, imaging alone will not be satisfactory in when setting out to unravel the origins of the local damage initiation mechanisms. To this end, local mechanical testing of the plasticity of indidivual phases and interfaces is required. Over the last years, micromechanical methods have been developed which have the potential to achieve this. We therefore also apply microcantilever bending tests to illustrate the extension of microscopic observation towards microscopic mechanical characterization to ultimately enable a mechanism-based understanding of damage that will allow purposeful tailoring of microstructures including their local mechanical properties to delay or prevent the accumulation of damage and the formation of catastrophic damage events during forming and application.

In the following, we will intitially describe each of the light and electorn microscopy methods employed for microscale quantification of deformation- and inclusion-induced damage. Finally, we present micro-cantilever bending as a method which will allow the extension of microscopic observation towards correlative micromechanical testing. For all characterization experiments, a single sample of a commercial dual phase DP800 steel was used. This ensures direct comparability of results and allows us to discuss the advantages and disadvantages of each method as well as their limitations.

2 Methods of microscale damage quantification

Of the various methods commonly used for imaging and characterization of microstructural voids, this work focuses on direct, metallographical investigation of planar samples

to characterize microstructural damage in the form of deformation-induced voids (in contrast to voids induced by prior processing steps or inclusions). The classically applied method of light microscopy is compared to two state-of-the-art SEM-based approaches, one relying on analytical, energy-dispersive X-ray spectroscopy (EDX) to characterize the origin of voids, and the other applying a deep-learning approach using convolutional neural networks to distinguish between void initiation mechanisms. Both methods operate with the same spatial resolution (32 nm/px), while maintaining the ability to image large areas of several hundred μm^2, due to automation of image acquisition, void identification, damage classification and data processing. Here, all investigations have been carried out on the same, polished surface of a commercial DP800 steel grade deformed in tensile loading to 14% strain, so that the obtained results from each method can be directly compared.

2.1 Light microscopy

Light microscopy is widely used for damage assessment, as it is a readily available method in any metallographic laboratory. To detect small, deformation-induced voids, specific sample preparation routines are necessary to reveal voids created during processing. Usually, for light microscopy, samples are ground in several steps, each reducing the coarseness of the grinding paper, and afterwards polished with diamond paste using a particle diameter of the order of 1 µm. If the material's microstructure is of interest, the specimen is then etched for observation to reveal individual phases or grain boundaries. For observation of voids, a polished sample is used, since on a clear surface, voids (and inclusions) will show as black dots. However, this preparation method is problematic, since during sample preparation, the voids may be covered with material removed elsewhere on the surface. Thus, after polishing a separate step is needed, that commonly involves immersion in an etching agent.. Here, the material is etched for a very short time between 1 and 3 s in 1% Nital. Afterwards, the specimen is, again, polished. This intermediate etching dissolves the material covering the voids and thus makes them detectable under light optical microscopes.

After the sample is prepared as described above, it is possible to analyze the state of the sample in terms of its void content with minimal contrast from the underlying microstructure. In Fig. 1a), a typical image of a sample prepared by intermediate etching can be seen. The differentiation between voids and inclusions cannot be made by light microscopy, as the observed black areas can be both voids or inclusions. Since most of the sampled areas are large enough (multiple µm in diameter) it is to be expected, that a large proportion of these areas are formed around inclusions, and do not correspond to deformation-induced voids.

Since this method allows inspection of a large area within a small timeframe, it is considered suitable for qualitative analysis of the damage state, while for a quantitative analysis the following SEM-based methods are more apt.

In addition, it is important to choose the magnification for the analysis very carefully to balance speed and detail of examination, bearing in mind that a qualitative or comparative determination of damage is usually the main objective in light microscopy.

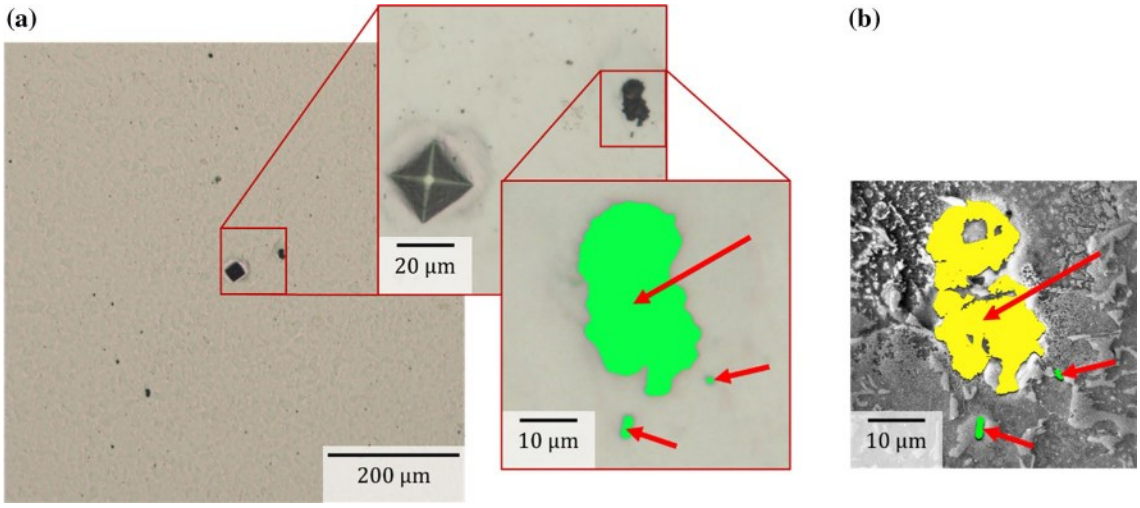

Fig. 1 **a** Identification of voids by light microscopy (voids identified in green), and **b** by SEM allowing separation of deformation-induced voids from inclusions (yellow) (color figure online)

2.2 Automated SEM and damage analysis using deep learning

To realize a significantly higher spatial resolution, SEM is applied to resolve all voids down to the sub-µm scale contained in the microstructure. Statistical relevance, however, has to be maintained to gather meaningful data about void size and the overall state of damage in the observed specimen. Therefore, an automated panoramic imaging approach [11] (Fig. 2) using a Zeiss Leo 1530 FEG-SEM (Carl Zeiss Microscopy GmbH, Jena, Germany) is chosen here to obtain micrographs with 32 nm/px resolution. The panoramicimage is stitched together from individual, overlapping images via a Matlab script based on VLFeat image toolbox [27]. The images are obtained using secondary electron detection.

To unravel dominant damage mechanisms in a specific sample, statistically sound data needs to be obtained, leading to a large amount of voids to be classified according to their mechanisms of initiation. As morphological differences visible in SEM images typically set apart these damage mechanisms, using deep-learning based image recognition and analysis tools is regarded as a drastic improvement in efficiency compared to a manual classification. Furthermore, no variations between the evaluating person have to be considered when automating the process. In this way, consistent data can be obtained from large sample areas while minimizing the time needed for evaluation. The steps of void recognition, and further analysis are depicted in Fig. 2. The images are processed using a grayscale cut-off coupled to a clustering algorithm [28] so that voids are identified as black clusters and individually processed as tensors of the size (250,250,1), corresponding to a 250 px wide square around the detected void. The detected voids are then entered into a first convolutional neural network trained to identify voids caused by inclusions. For this purpose, the network Inception V3 [29] is used. Thus, for DP steels in this case, all voids caused by inclusions can be disregarded for measurements of deformation-induced damage. The error made when considering the area or site fraction of all voids, i.e. deformation- and inclusion induced together, can, therefore, be calculated. It has been shown to reach values of the order of 50% at low strains, where inclusion voids naturally dominate, and diminish at high strains once the deformation-induced damage fraction becomes large [11].

Where the underlying mechanisms of damage initiation are of interest, a second convolutional neural network is used and trained to further classify the deformation-induced voids with respect to their mechanisms of initiation. As deformation-induced voids are typically smaller than inclusions, the processed tensors are cropped to a size of (50,50,1) around the void for this process step. Subsequently, all deformation-induced voids are passed over to a watershed algorithm to

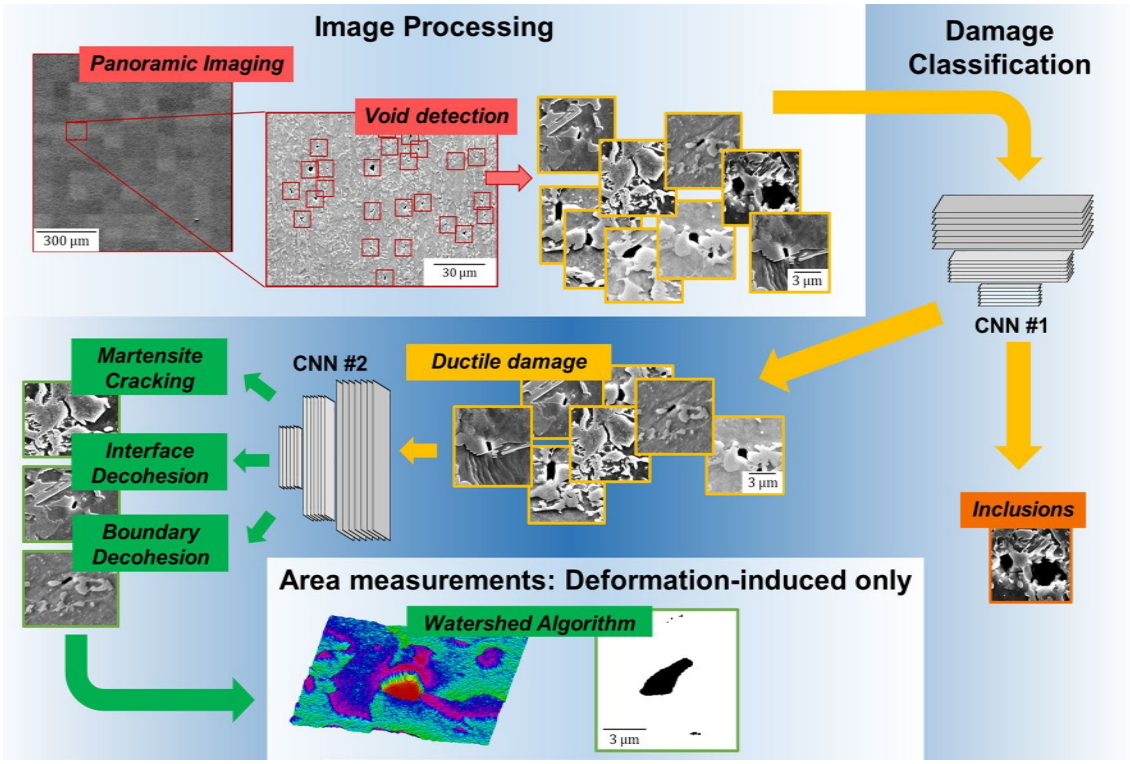

Fig. 2 Void recognition, classification and area measurement approach for panoramic SE-images using deep learning for damage classification (*CNN* convolutional neural network). Adapted from [11]

measure their area individually, so that detailed area statistics of void origin and size are obtained concurrently. The method is described in more detail in [11] and has also been applied to statistically assess damage formation on the scale of bent sheet metal samples formed using two different bending processes [30]. The accuracy for the first network, that is used in this work, reached an accuracy of $95 \pm 1\%$, trained on a total of 4944 damage and inclusion sites and tested on 20% of these as test data.

2.3 Automated particle analysis by EDX

To distinguish deformation-induced voids from inclusion-induced voids, the analytical method of EDX can also be used, equally coupled to an automated SEM-based image acquisition tool. This approach additionally reveals information about the chemistry of the material forming the inclusion by the obtained spectra.

Here, the damage quantification using automated EDX particle analysis was performed in a JEOL JSM 7000F FEG-SEM (JEOL, Akashima, Japan) using the particle analysis software EDAX Genesis (Version 6.53, EDAX, New Jersey, USA). Backscatter electron images are used due to the good element contrast. Grayscale thresholds are selected to detect all types of inclusion and voids. After image acquisition and detection of voids and inclusions, EDX measurements are performed on every detected object using automatic stage shifts to allow investigation of large areas. After the measurement finished, the element information is combined with the information obtained by the image to identify voids, different types of inclusions and also preparation artifacts. Additionally, morphology data, such as area or average diameter are obtained.

Figure 3 exemplifies the steps in the used methodology: first, a backscattered-electron (BSE) image is collected, which subsequently undergoes a greyscale analysis. Two different greyscale ranges are detected, the darkest regions are marked in yellow, intermediate greyscales are marked in green. As next step, EDX spectra are collected from all marked objects. These steps are repeated in an automated process to investigate larger areas. After all images and spectra are recoreded, the objects are classified. An example of this classification is shown in step 3 of Fig. 3. Even though both spectra show characteristic x-ray lines of elements present in inclusion and matrix, the combination of BSE greyscale and EDX spectrum leads to the classification result. In the case shown in Fig. 3, the yellow region is interpreted as a void in between two parts of a cracked TiN particle.

3 Results from void measurements

For all three applied microscopic void analysis methods, the same area with a size of 700×700 µm was analyzed, and no further preparation apart from etching for the SEM panoramic imaging approach was undertaken, so that results are comparable. The field of view was identified using a central indentation that was removed from the images before further

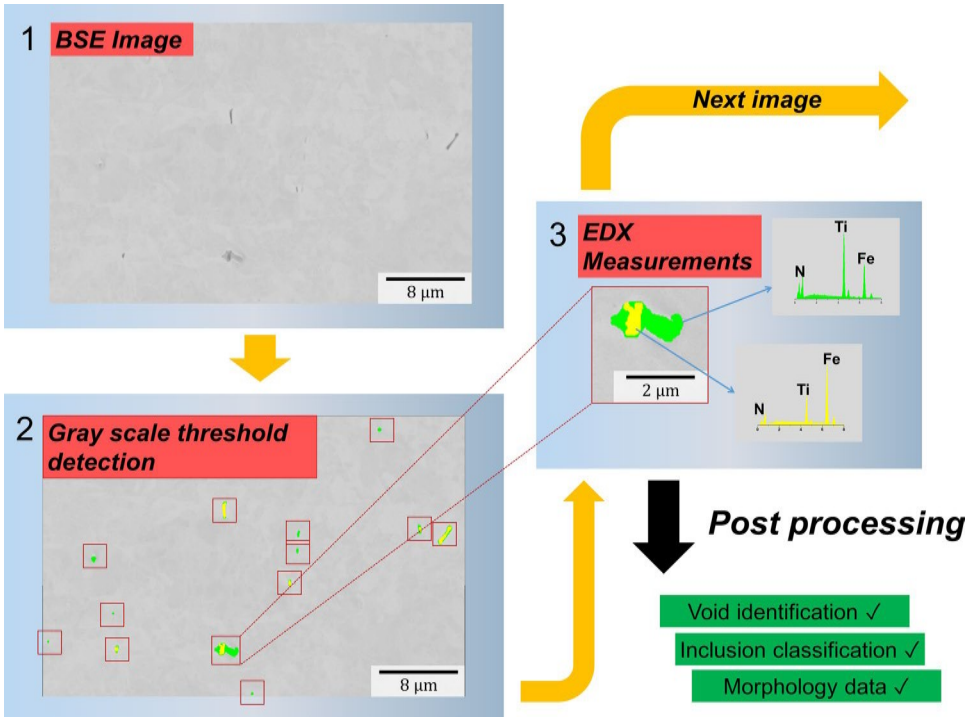

Fig. 3 Automated EDX particle analysis coupled to void recognition and area measurements

processing. Table 1 lists the overall void numbers, total void area and area fraction obtained for the three methods. As for dual-phase steels, the fundamental damage mechanisms originate from the mechanical contrast between ferrite and martensite, observed voids that have been classified as inclusions by the respective methods have not been considered for these statistics of deformation-induced damage.

While the detected number of voids is, with a deviation in area fraction of 2%, comparable for the SEM-based methods, the lower-resolution light optical analysis shows a clear difference in the number of detected voids with 376 total voids, only about a third of the number of voids detected by SEM. However, the measured area fraction shows a contrary behavior: Here, the measured area is significantly higher for the analysis by light microscopy with a measured area (fraction) more than three times that measured by the SEM-based methods. This trend is equally shown in a comparison of cumulative void area as a function of individual void area, as shown in Fig. 4. As cumulative statistics, scaled with the void area, clearly show the contribution of the increasing void sizes to the overall outcome in measured void area, these have been chosen to illustrate the different detection behavior of the used methods.

Here, all three methods show a similar behaviour for small voids ($<3\ \mu m^2$) with the optical microscope expectedly giving lower values than the SEM-based methods. For larger voids above 10 µm, optical microscopy suggests much larger void areas and a dominance of large void sizes. However, this is to be considered an artefact of the method as these large voids are typically caused only by inclusions. Using the SEM-based methods, these are readily recognized and can be treated separately from the deformation-dependent changes in void area.

As shown in Fig. 5, the SEM-based methods give similar measurements of total void area, but with slight variations in the cumulative void area as a function of individual void size. The SE + Deep Learning approach detects more voids in the range of 0.5 to 1.5 μm^2, while the EDX particle analysis data yields more voids larger than 3 μm^2, with the maximum void size being 11.1 μm^2. As such a large void could be expected to be at an inclusion, the largest detected void was chosen for direct comparison between the two methods,

Table 1 Number, total area and area fraction of voids as detected by each microscopy method

	Number	Total area in μm^2	Area fraction
SE + deep learning	1128	255.15	5.2×10^{-5}
EDX analysis	1266	250.87	5.1×10^{-5}
Light microscopy	376	824.00	16.8×10^{-5}

Note that in the case of both SEM-based methods, the measurements have been corrected to exclude inclusions

Fig. 6b). Additionally, two smaller voids are shown in Fig. 6, and their measured areas are compared.

As shown, the largest void observed by the particle analysis is indeed due to an inclusion which was removed during surface preparation. As the inclusion is no longer present, elements not present in the matrix could only be detected across parts of the void. In the EDX analysis, the whole arrangement is therefore counted as a mixture of inclusion and void. In contrast, the deep learning algorithm, which relies on morphological appearance only, correctly classifies this void in its entirety as an inclusion and therefore avoids this error in classification and measurement. A difference of 3% in terms of measured void area results between the two methods. The voids in Fig. 6a, c show correct classification by both the deep learning analysis as well as the EDX particle analysis. As one of the most dominant damage initiation mechanisms, martensite cracks like this are of particular interest in terms of characterizing site-specific microstructural damage processes. To determine critical cracks and subsequently correlate these to the measured void data, this mechanism will be regarded further using micro-cantilever experiments.

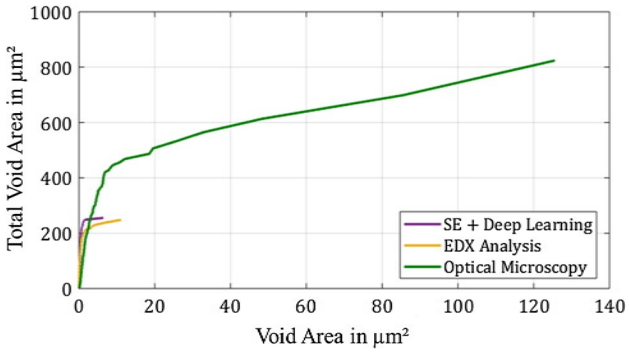

Fig. 4 Cumulative void area versus individual void area for SEM-based and optical measurements

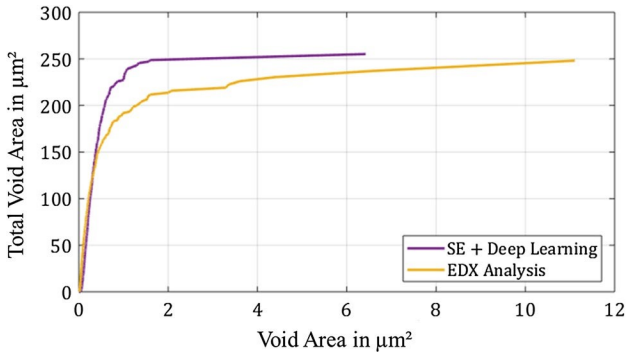

Fig. 5 Cumulative void area versus individual void size for the SEM-based void characterization tools only

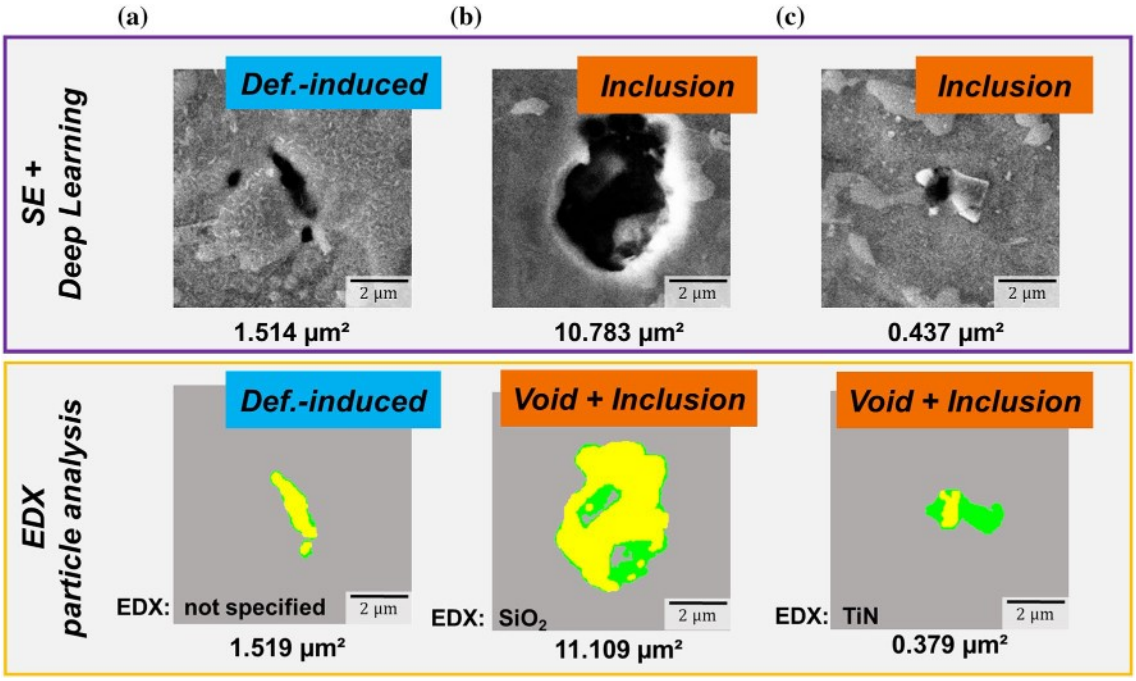

Fig. 6 Comparison of results for classification of voids based on deep learning and EDX analysis. **a** Void classified correctly by both approaches as deformation-induced damage and further identified as a martensite crack by the deep learning approach, **b** void classified as inclusion by deep learning, and as mixture of void and inclusion by EDX, **c** void classified as cracked inclusion by both approaches

4 Micro-cantilever testing

To set the statistics of deformation-induced void sizes into perspective to a critical void size for fracture of the brittle microstructure constituents and interfaces, we used the method of micro-cantilever bending.

Within this work, we are in particular interested in the fracture toughness of martensite islands, non-metallic inclusions and interfaces between martensite and ferrite, corresponding to the main damage initiation mechanisms. The example in Fig. 7 shows a micro cantilever consisting of martensite, produced by focused ion beam (FIB) milling [31–34]. It is designed in such a way that only the gauge region close to the notch is a martensite island, and the entire thick portion of the cantilever is a mixture of ferrite and martensite. This geometry is required to suppress plasticity in ferrite and force the crack to grow inside the martensite. The micro cantilevers are further tested in situ in an SEM (Gemini 500, Carl Zeiss Microscopy GmbH, Jena, Germany)—as exemplarily shown on the same martensite island in Fig. 7. The load displacement signal is recorded simultaneously with SEM images using an Asmec Unat II indenter (ASMEC GmbH, Dresden, Germany) equipped with a 10 µm sized conductive diamond wedge.

From both, the force–displacement signal as well as from the snapshots presented in Fig. 7, the elasto-plastic crack propagation is evident. A thorough analysis of the crack resistance curve—as for instance provided in references [35, 36]—is needed to interpret the elasto-plastic fracture. For this purpose, several loading–unloading cycles were applied to measure the system compliance and derive the crack extension, required for elasto-plastic fracture mechanics.

However, for simplicity, we do not analyze the elasto-plastic fracture within this work and refer the reader to a thorough investigation provided elsewhere. Instead, we focus on the analysis of the linear elastic fracture mechanics and, as our curve shows significant plasticity around the crack tip, we will analyze the conditional toughness K_Q at which the crack starts to grow (see Eq. 1a below). The corresponding geometry factor was calculated by Matoy et al. [31], with F_Q as the load at which crack growth starts, L, B and W the bending length, the cantilever width and height respectively, and a the crack length. The ratios $W{:}B{:}L{:}a$ were maintained throughout all experiments and are 1:1:5:0.2, according to [37, 38]. The sample height W is limited by the size of the martensitic island, and was typically smaller than 1 µm for the DP800 steel investigated here.

$$K_Q = \frac{F_Q L}{\mathrm{BW}^{3/2}} \cdot f\left(\frac{a}{W}\right) \tag{1a}$$

$$f\left(\frac{a}{W}\right) = 1.46 + 24.36\left(\frac{a}{W}\right) - 47.21\left(\frac{a}{W}\right)^2 + 75.18\left(\frac{a}{W}\right)^3 \tag{1b}$$

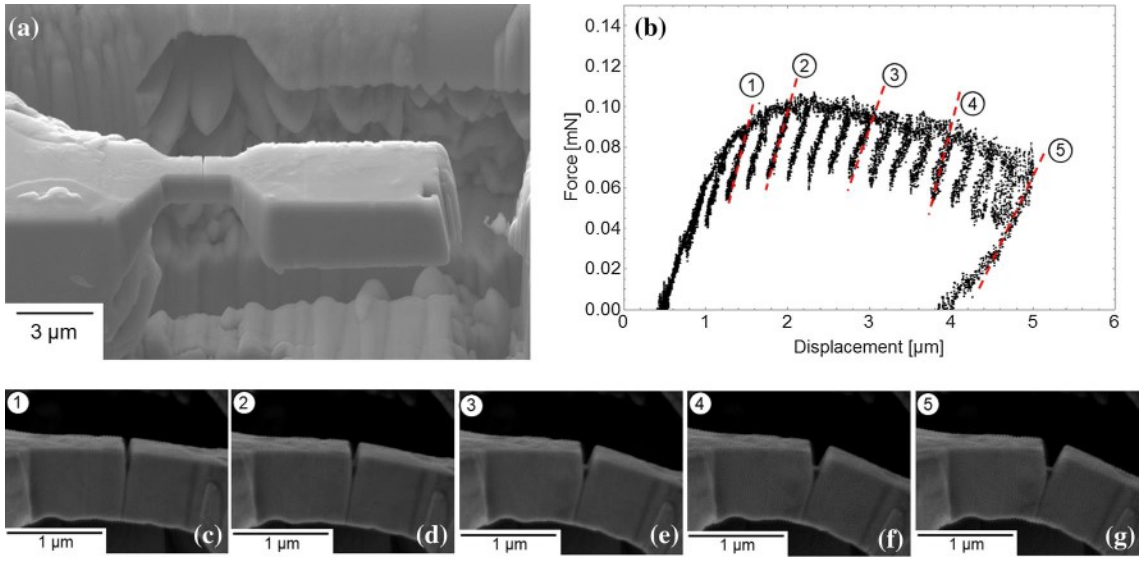

Fig. 7 **a** Micro-cantilever prepared for analyzing the fracture toughness of a martensite island. **b** The load–displacement curve of the bending test with several indicated unloading segments. **c–g** SEM snapshots of the martensite island to monitor crack growth. The numbers correlate the snapshots to the force–displacement curve in **b**

The force at which crack growth was observed is 0.080 ± 0.005 mN in the example presented in Fig. 7. By applying Eq. (1) and using the geometry of our bending cantilever, we can compute a conditional toughness of 2.4 ± 0.2 MPa $m^{1/2}$. It is noted that this is a lower bound value for the fracture toughness of the investigated phase and a thorough analysis of the crack resistance curve and the *J* integral is required for comparison with macroscopic toughness (cf. work on nanocrystalline ferrite in [39]).

5 Discussion

In this work, we presented two SEM-based approaches to reliably and efficiently characterize void formation events in a statistically sound way. This was demonstrated using a commercial dual-phase steel subjected to tensile testing as an example. Compared to the more classical analysis of voids via metallographic preparation and subsequent light microscopy, these methods showed a clearly obtainable improvement detecting more, and foremost, smaller voids. While light microscopy is able to detect deformation-induced voids, the higher-resolved SEM imaging methods show that a much more quantitative approach to considering all deformation-induced voids can be executed using higher-resolved SEM methods. This is due to two factors: The much improved resolution of the SEM in comparison to light microscopy and, for these novel approaches, the ability to maintain the large field of view without introducing the requirement for regularly inaccessible or unfeasible methods or equipment in the measurement process. Even in comparison with statistical approaches to microscale damage as by Hoefnagels et al. [8], the field of view could be drastically enlarged by not only detecting voids in an automated way [12], but also applying automated classification of the observed voids [11]. Differences in the classification between the analytical EDX approach and the deep-learning-based image recognition approach were suspected from the statistics shown in Fig. 5 and equally found in the classification of voids as inclusions (Fig. 6). As the EDX particle analysis is able to split between an inclusion and void partition of a site, whereas the deep-learning method distinguishes between inclusions and deformation-induced voids only, these differences in classification can lead to an advantage in accuracy for one of the two methods, depending on the material and its mechanisms of damage formation. When deformation-induced damage mechanisms are based on strain partitioning Other approaches have been performed for microstructural classification to microstructural features like phases and their distribution [16]. However, here, we apply automation in a site-specific way to directly characterize many individual damage events. The main benefit of applying both presented approaches can therefore be found in the interplay of deep learning based algorithms that are capable of reliably classifying the detected microstructural features, and the presented analytical approach, combining automated void detection with analytical detectors like EDX. In this way, it is now possible to achieve a massively enlarged statistical relevance for microscale damage events, but coupled to an improved efficiency, that makes these high-resolution approaches applicable for assessments of damage processes in formed macrosocopic components [30] rather

than micro-scale specimens only. Light microscopy can, as it resolves the larger deformation-induced voids, deliver a qualitative picture of the state of damage to the microstructure when efficient handling is a priority.

Combining these findings on void sizes and the local mechanical data of microstructural elements obtained from micro-cantilever bending experiments yields a thorough picture about the impact of void initiation and growth in dual or multi phase materials. This approach can easily be transferred to any material composite with pronounced mechanical heterogeneity, such as alloys with intermetallic skeletons or large, hard particles [40].

The knowledge of a statistically sound void size distribution is equally critical for constructing a realmicrostructure-based representative volume element and conducting crystal plasticity finite element modeling (CP-FEM). The micro cantilever fracture experiments—which result in a conditional fracture toughness or even crack resistance curve of individual grains, phases or interfaces—can finally be used to predict void nucleation and growth. Besides this predictive capabilities the combined method of analyzing pore size distributions and toughness evaluation will allow for the numerical optimization of damage tolerant microstructures or forming processes suppressing damage.

6 Conclusion and outlook

We presented here a statistical approach to deformation-induced damage, enabled by the use of experimental and analytical automation in two SEM-based analyses employing additional EDX data or a deep learning based classification of images. Both methods were shown to deliver larger and more statistically sound data from sample areas of technological relevance. They were in particular compared with each other and with light microscopy, as the typically employed method for large area characterization:

- With deviations in the range of few %, the two proposed automated SEM-imaging approaches can reliably detect and quantify the smaller (< 1 µm) while maintaining experimental efficiency due to their high level of automation.
- The additional characterization by means of EDX and deep-learning based classification allows separation of deformation- and inclusion induced voids.
- Light microscopy cannot to resolve the majority of deformation-induced voids to accurately quantify their area or unravel their mechanisms of origin, and can therefore only serve as a quick and efficient tool to qualitatively characterize damage in the examined dual-phase steel grade.

In the future, the results from micro-cantilever characterization of local fracture properties can be correlated with the void area statistics from the two imaging methods to gain a deeper understanding of the critical size and impact of voids on the microstructural behavior. For ductile microstructure constituents, the presented linear elastic model will have to be extended to elasto-plastic fracture mechanics and the micro-fracture testing supplemented by other micromechanical methods measuring the resistance to plastic flow, e.g. nanoindentation or microcompression. These coupled results about the fracture behavior of microstructural constitutents and statistical information about damage sites, quantity and spatial distribution are valuable data for both microscale damage modelling approaches as well as technological developments of damage-tolerant materials and process design.

Even without direct coupling to local mechanical testing, the presented characterization tools using automated imaging at high resolution, void recognition and classification will now enable more detailed studies of void formation on a technologically and statistically relevant scale to not only lead to new insights into fundamental damage mechanisms but their impact on the material behaviorand the resulting properties of products after forming.

Acknowledgements The investigations are kindly supported by the German Research Foundation in context of the Collaborative Research Centre CRC/Transregio 188 “Damage-Controlled forming processes”, projects B02, B03, B04 and B05. The Funding has been received from Deutsche Forschungsgemeinschaft with Grant No. 278868966.

Compliance with ethical standards

Conflict of interest The authors declare no conflict of interest.

References

1. Calcagnotto M, Ponge D, Demir E, Raabe D (2010) Orientation gradients and geometrically necessary dislocations in ultrafine grained dual-phase steels studied by 2D and 3D EBSD. Mater Sci Eng, A 527:2738–2746
2. Bleck W, Papaefthymiou S, Frehn A (2004) Microstructure and tensile properties in dual phase and trip steels. Steel Res Int 75(11):704–710
3. Davies R (1978) Influence of martensite composition and content on the properties of dual phase steels. Metall Trans A 9(5):671–679
4. Calcagnotto M, Adachi Y, Ponge D, Raabe D (2011) Deformation and fracture mechanisms in fine. and ultrafine-grained ferrite/martensite dual-phase steels and the effect of aging. Acta Mater 59:658–670
5. Tasan CC, Hoefnagels JPM, Diehl M, Yan D, Roters F, Raabe D (2014) Strain localization and damage in dual phase steels investigated by coupled in situ deformation experiments and crystal plasticity simulations. Int J Plast 63:198–210

6. Kadkhodapour J, Butz A, Rad SZ (2011) Mechanisms of void formation during tensile testing in a commercial, dual-phase steel. Acta Mater 59:2575–2588
7. Lai Q, Bouaziz O, Gouné M, Brassart L, Verdier M, Parry G, Perlade A, Bréchet Y, Pardoen T (2015) Damage and fracture of dual-phase steels: influence of martensite volume fraction. Mater Sci Eng, A 646:322–331
8. Hoefnagels JPM, Tasan CC, Maresca F, Peters FJ, Kouznetsova VG (2015) Retardation of plastic instability via damage-enabled microstrain delocalization. J Mater Sci 50:6882–6897
9. Tekkaya AE, Khalifa NB, Hering O, Meya R, Myslicki S, Walther F (2017) Forming-induced damage and its effects on product properties. CIRP Ann 66(1):281–284
10. Kadkhodapour J, Butz A, Ziaei-Rad S, Schmauder S (2011) A micro mechanical study on failure initiation of dual phase steels under tension using single crystal plasticity model. Int J Plast 27:1103–1125
11. Kusche C, Reclik T, Freund M, Al-Samman T, Kerzel U, Korte-Kerzel S (2019) Large-area, high-resolution characterisation and classification of damage mechanisms in dual-phase steel using deep learning. PLoS One 14(5):e0216493
12. Aşık E, Perdahcıoğlu E, van den Boogaard A (2019) Microscopic investigation of damage mechanisms and anisotropic evolution of damage in DP600. Mater Sci Eng A 739:348–356
13. Landron C, Maire E, Bouaziz O, Adrien J, Lecarme L, Bareggi A (2011) Validation of void growth models using X-ray microtomography characterization of damage in dual phase steels. Acta Mater 59(20):7564–7573
14. Maire E, Withers PJ (2014) Quantitative X-ray tomography. Int Mater Rev 59(1):1–43
15. Morgeneyer TF, Helfen L, Mubarak H, Hild F (2013) 3D digital volume correlation of synchrotron radiation laminography images of ductile crack initiation: an initial feasibility study. Exp Mech 53(4):543–556
16. Azimi SM, Britz D, Engstler M, Fritz M, Mücklich F (2018) Advanced steel microstructural classification by deep learning methods. Sci Rep 8:2128
17. Korte S, Ritter M, Jiao C, Midgley P, Clegg W (2011) Three-dimensional electron backscattered diffraction analysis of deformation in MgO micropillars. Acta Mater 59(19):7241–7254
18. Dehm G, Jaya BN, Raghavan R, Kirchlechner C (2018) Overview on micro-and nanomechanical testing: new insights in interface plasticity and fracture at small length scales. Acta Mater 142:248–282
19. Korte-Kerzel S (2017) Microcompression of brittle and anisotropic crystals: recent advances and current challenges in studying plasticity in hard materials. MRS Commun 7(2):109–120
20. Pippan R, Wurster S, Kiener D (2018) Fracture mechanics of micro samples: fundamental considerations. Mater Des 159:252–267
21. Durst K, Maier V (2015) Dynamic nanoindentation testing for studying thermally activated processes from single to nanocrystalline metals. Curr Opin Solid State Mater Sci 19(6):340–353
22. Gibson JS-L, Schröders S, Zehnder C, Korte-Kerzel S (2017) On extracting mechanical properties from nanoindentation at temperatures up to 1000 C. Extreme Mech Lett 17:43–49
23. Wheeler J, Armstrong D, Heinz W, Schwaiger R (2015) High temperature nanoindentation: the state of the art and future challenges. Curr Opin Solid State Mater Sci 19(6):354–366
24. Korte S, Stearn RJ, Wheeler JM, Clegg WJ (2012) High temperature microcompression and nanoindentation in vacuum. J Mater Res 27(1):167–176
25. Tasan CC, Diehl M, Yan D, Zambaldi C, Shanthraj P, Roters F, Raabe D (2014) Integrated experimental-simulation analysis of stress and strain partitioning in multiphase alloys. Acta Mater 81:386–400
26. Ramanzani AS, Aretz A, Prahl U, Bleck W (2013) Characterization and modelling of failure initiation in DP Steel. Comput Mater Sci 75:35–44
27. Vedaldi A, Fulkerson B (2008) VLFeat: an open and portable library of computer vision algorithms. http://www.vlfeat.org/
28. Sander J, Ester M, Kriegel H-P, Xu X (1998) Density-based clustering in spatial databases: the algorithm GDBSCAN and its applications. Data Min Knowl Disc 2(2):169–194. https://doi.org/10.1023/a:1009745219419
29. Szegedy C, Vanhoucke V, Ioffe S, Shlens J, Wojna Z (2016) Rethinking the inception architecture for computer vision. In: Proceedings of the IEEE conference on computer vision and pattern recognition, pp 2818–2826
30. Meya R, Kusche CF, Löbbe C, Al-Samman T, Korte-Kerzel S, Tekkaya AE (2019) Global and high-resolution damage quantification in dual-phase steel bending samples with varying stress states. Metals 9(3):319
31. Matoy K, Schönherr H, Detzel T, Schöberl T, Pippan R, Motz C, Dehm G (2009) A comparative micro-cantilever study of the mechanical behavior of silicon based passivation films. Thin Solid Films 518(1):247–256. https://doi.org/10.1016/j.tsf.2009.07.143
32. Di Maio D, Roberts SG (2011) Measuring fracture toughness of coatings using focused-ion-beam-machined microbeams. J Mater Res 20(02):299–302. https://doi.org/10.1557/jmr.2005.0048
33. Jaya BN, Kirchlechner C, Dehm G (2015) Can microscale fracture tests provide reliable fracture toughness values? A case study in silicon. J Mater Res 30(5):686–698. https://doi.org/10.1557/jmr.2015.2
34. Jaya BN, Wheeler JM, Wehrs J, Best JP, Soler R, Michler J, Kirchlechner C, Dehm G (2016) Microscale fracture behavior of single crystal silicon beams at elevated temperatures. Nano Lett 16(12):7597–7603. https://doi.org/10.1021/acs.nanolett.6b03461
35. Wurster S, Motz C, Pippan R (2012) Characterization of the fracture toughness of micro-sized tungsten single crystal notched specimens. Philos Mag 92(14):1803–1825
36. Ast J, Göken M, Durst K (2017) Size-dependent fracture toughness of tungsten. Acta Mater 138:198–211. https://doi.org/10.1016/j.actamat.2017.07.030
37. Brinckmann S, Kirchlechner C, Dehm G (2017) Stress intensity factor dependence on anisotropy and geometry during microfracture experiments. Scripta Mater 127:76–78. https://doi.org/10.1016/j.scriptamat.2016.08.027
38. Brinckmann S, Matoy K, Kirchlechner C, Dehm G (2017) On the influence of microcantilever pre-crack geometries on the apparent fracture toughness of brittle materials. Acta Mater 136:281–287. https://doi.org/10.1016/j.actamat.2017.07.014
39. Jaya BN, Goto S, Richter G, Kirchlechner C, Dehm G (2017) Fracture behavior of nanostructured heavily cold drawn pearlitic steel wires before and after annealing. Mater Sci Eng, A 707:164–171. https://doi.org/10.1016/j.msea.2017.09.010
40. Zubair M, Sandlöbes S, Wollenweber M, Kusche C, Hildebrandt W, Broeckmann C, Korte-Kerzel S (2019) On the role of Laves phases on the mechanical properties of Mg–Al–Ca alloys. Mater Sci Eng, A 756:272–283